Supplementary Material

Removal of Aniline and Benzothiazole Wastewaters Using an Efficient MnO2/GAC Catalyst in a Photocatalytic Fluidised Bed Reactor

Cristian Ferreiro [1,*], Natalia Villota [2], José Ignacio Lombraña [1], María J. Rivero [3], Verónica Zúñiga [4] and José Miguel Rituerto [4]

[1] Department of Chemical Engineering, Faculty of Science and Technology, University of the Basque Country UPV/EHU, Barrio Sarriena s/n, 48940 Leioa, Spain; ji.lombrana@ehu.eus

[2] Department of Chemical and Environmental Engineering, Faculty of Engineering Vitoria-Gasteiz, University of the Basque Country UPV/EHU, Nieves Cano 12, 01006 Vitoria-Gasteiz, Spain; natalia.villota@ehu.eus

[3] Department of Chemical and Biomolecular Engineering, University of Cantabria, 39005 Santander, Spain; riveromj@unican.es

[4] General Química, S.A.U. (Grupo Dynasol), 01213 Lantaron, Spain; veronica.zuniga@repsol.com (V.Z.); jrituertol@repsol.com (J.M.R.)

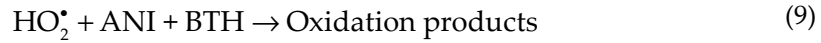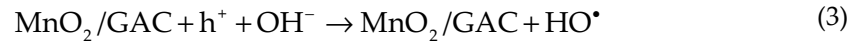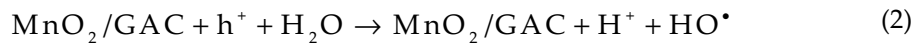* Correspondence: cristian.ferreiro@ehu.eus; Tel.: +34-946-012-512

Table S1. Previous studies of photocatalysis using manganese oxides supported on carbonaceous materials.

Catalyst	Operating conditions	Comments	Ref.
α-MnO$_2$	$[Cat.] = 0.025$ g $\tau = 1.655 \times 10^{-3}$ mol h^{-1} g cat^{-1} $T = 25$ °C $Time = 8$ h $[\% \ removal] = 100$	Up to 100% conversion into acetone using an amorph MnO$_2$ photocatalytic system for 2-propanol removal. The α-MnO$_2$ phase was more active and regenerable than other manganese oxides.	[1]
α-MnO$_2$/CNT	$[Cat.] = 0.4$ g L^{-1} $C_0 = 20$ mg L^{-1} $T = 25$ °C $Time = 75$ min $[\% \ removal] = 24$	Compared different crystalline phases of MnO$_2$. Found that α-MnO$_2$ particles supported on carbon nanotubes (CNT) improved the surface area of the hybrid structure and had a better performance under visible light.	[2]
MnO$_2$/AC	$[Cat.] = 3.0$ g L^{-1} $C_0 = 60$ mg L^{-1} $T = 25$ °C $Time = 5$ min $[\% \ removal] = 98.53$	Compared the catalytic activity of MnO$_2$ nanoparticles to that of MnO$_2$/AC composites. The composite removed 31.96% more Congo Red (CR) dye than the nanoparticles. The presence of mineral ions led to a higher dye degradation rate.	[3]
GO/MnO$_2$	$[Cat.] = 0.5$ g L^{-1} $C_0 = 60$ mg L^{-1} $T = 25$ °C $Time = 120$ min $[\% \ removal] = 98$	Observed that the catalytic activity during Reactive Black 5 (RB5) removal was higher than that of their starting materials. The presence of graphene oxide with a 20% MnO$_2$ content helped to increase the generation of hydroxyl radicals and facilitated their separation from the solution, in contrast to MnO$_2$ nanoparticles.	[4]
MnO$_2$/AC	$[Cat.] = 0.5$ g L^{-1} $C_0 = 100$ mg L^{-1} $T = 25$ °C $Time = 60$ min $[\% \ removal] = 85$	Impregnated an activated carbon with a 20% BMnO$_2$ content. Concluded that carbon impregnated with BMnO$_2$ showed a higher potential for RB5 degradation.	[5]

Photocatalytic reaction mechanism with MnO₂/GAC composites

The improvement can be attributed to the reaction mechanisms which occur on the surface of the catalyst. The trigger mechanism begins with light absorption (hv), generating electron-hole (e⁻ - h⁺) pairs, which act as reducing and oxidising agents (Eq. 1). During oxidation, water (Eq. 2) or hydroxide ions (OH⁻) (Eq. 3) adsorbed on the catalyst generate hydroxyl radicals (HO•), while oxygen prevents the recombination of electron-hole pairs (Eq. 4). Subsequently, when irradiating a photon of energy equal to or greater than the band gap energy, the excitation of electrons in the conduction band (CB) is produced and it generates an equal number of holes in the valence band (VB) (Eqs. 5– 7). At that point, Eqs. 8–9, the high oxidative species generated are responsible for ANI and BTH oxidation to other degradation by-products.

According to Ameta [6] and Rahmat et al. [7], the equations below describe a plausible mechanism of photocatalysis of an activated carbon material modified with MnO₂ (MnO₂/GAC):

$$MnO_2/GAC \xrightarrow{\text{h}v} MnO_2/GAC \left(e^- + h^+\right) \tag{1}$$

$$MnO_2/GAC + h^+ + H_2O \rightarrow MnO_2/GAC + H^+ + HO^\bullet \tag{2}$$

$$MnO_2/GAC + h^+ + OH^- \rightarrow MnO_2/GAC + HO^\bullet \tag{3}$$

$$MnO_2/GAC + e^- + O_2 \rightarrow MnO_2/GAC + O_2^{-\bullet} \tag{4}$$

$$O_2^{-\bullet} + H^+ \rightarrow HO_2^\bullet \tag{5}$$

$$HO_2^\bullet + HO_2^\bullet \rightarrow H_2O_2 + O_2 \tag{6}$$

$$H_2O_2 \xrightarrow{\text{h}v} HO^\bullet \tag{7}$$

$$HO^\bullet + ANI + BTH \rightarrow Oxidation\ products \tag{8}$$

$$HO_2^\bullet + ANI + BTH \rightarrow Oxidation\ products \tag{9}$$

Achieving a high removal efficiency during the photocatalytic process requires [8–10]: i) an adequate diffusion of contaminants from the liquid phase to the surface of the MnO₂ catalyst, ii) a strong adsorption of organic pollutants on the surface of MnO₂, iii) redox reactions at the catalyst surface level, and iv) desorption of oxidation products. Based on these conditions, the reactor could play a key role not only in terms of degradation but also in terms of ANI and BTH mineralisation. Therefore, the application of advanced oxidation processes (AOPs) with suitable reactor technology can reduce catalyst damage whilst increasing reuse [11].

Analytical methods for influent characterization

Nitrite, nitrates, chlorides and phosphates were measured by ion chromatography (IC) using a Dionex Model 2010i Ion Chromatograh (Dionex, Sunnyvale, CA, USA) with a conductivity detector, Model CDM-1 (Dionex, Sunnyvale, CA, USA). Chromatographic separation was achieved using a IonPac-AS4 (250 × 4.0 mm, Dionex, Sunnyvale, CA, USA) column with a IonPac-AG4 guard column (50 × 4.0 mm, Dionex, Sunnyvale, CA, USA). The eluent used consisted in a mixture of 3.5 mM $NaHCO_3$ and 2.0 mM Na_2CO_3. A sample volume of 50 μL was injected according with the method described by Urasa and Ferede [12].

Quality assurance (QA) and quality control (QC) protocols

The protocols followed for the determination of the different parameters listed in Table 1 were described below. The samples were subjected to drastic conditions to acid hydrolysis (1N HCl), basic hydrolysis (1N NaOH), sunlight and temperature (30 °C). Subsequently, the amount recovered was determined in triplicate after 7 days.

Table S2. Limit of quantification values (LOQ) and limit of detection values (LOD) of different parameters.

Parameter	LOQ	LOD
Aniline (mg L^{-1})	0.01	30.0
Benzothiazole (mg L^{-1})	0.02	24.0
Nitrite (mg NO_2 L^{-1})	0.0010	50.0
Nitrate (mg NO_3 L^{-1})	0.0015	75.0
Chloride (mg Cl L^{-1})	0.003	80.0
Total phosphorus (mg P L^{-1})	0.002	32.0
Phosphates (mg PO_4 L^{-1})	0.001	46.0

Table S3. Linearity values of different parameters.

Parameter	Range	Regression equation	R^2
Aniline (mg L^{-1})	0.1-20.0	y = 3.780 x + 2.350	0.998
Benzothiazole (mg L^{-1})	0.1-20.0	y = 7.033 x + 8.196	0.998
Nitrite (mg NO_2 L^{-1})	0.002-0.1	y = 5.280 x + 3.040	0.993
Nitrate (mg NO_3 L^{-1})	0.002-4.0	y = 2.098 x + 9.636	0.998
Chloride (mg Cl L^{-1})	0.01-65.0	y = 2.558 x + 3.146	0.991
Total phosphorus (mg P L^{-1})	0.01-0.1	y = 3.973 x + 5.480	0.995
Phosphates (mg PO_4 L^{-1})	0.01-0.3	y = 3.108 x + 2.721	0.998

Table S4. Specificity values of different parameters.

Parameter	Condition	Amount added	Amount recovered	Degradation (%)
Aniline (mg L^{-1})	Acidic degradation	12.0	11.7	1.87
	Alkaline degradation	12.0	11.7	2.12
	Solar light	12.0	11.6	3.04
Benzothiazole (mg L^{-1})	Acidic degradation	12.0	11.8	1.15
	Alkaline degradation	12.0	11.9	0.71
	Solar light	12.0	11.8	0.98
Nitrite (mg NO$_2$ L^{-1})	Acidic degradation	0.050	0.049	1.54
	Alkaline degradation	0.050	0.048	2.2
	Solar light	0.050	0.048	2.03
Nitrate (mg NO$_3$ L^{-1})	Acidic degradation	1.50	1.47	1.64
	Alkaline degradation	1.50	1.44	3.72
	Solar light	1.50	1.48	0.99
Chloride (mg Cl L^{-1})	Acidic degradation	30.0	29.3	2.31
	Alkaline degradation	30.0	28.9	3.47
	Solar light	30.0	29.6	1.02
Total phosphorus (mg P L^{-1})	Acidic degradation	0.05	0.04	0.8
	Alkaline degradation	0.05	0.04	1.74
	Solar light	0.05	0.05	2.8
Phosphates (mg PO$_4$ L^{-1})	Acidic degradation	0.100	0.097	2.7
	Alkaline degradation	0.100	0.099	0.85
	Solar light	0.100	0.096	3.87

Table S5. Accuracy values of different parameters.

Parameter	Range	Recovery (Mean ± % RSD)
Aniline (mg L^{-1})	0.1-20.0	100.91 ± 0.024
Benzothiazole (mg L^{-1})	0.1-20.0	100.24 ± 0.030
Nitrite (mg NO$_2$ L^{-1})	0.002-0.1	100.14 ± 0.020
Nitrate (mg NO$_3$ L^{-1})	0.002-4.0	100.08 ± 0.007
Chloride (mg Cl L^{-1})	0.01-65.0	100.05 ± 0.026
Total phosphorus (mg P L^{-1})	0.01-0.1	100.32 ± 0.013
Phosphates (mg PO$_4$ L^{-1})	0.01-0.3	100.56 ± 0.011

Table S6. Precision values of different parameters.

Parameter	Concentration	Standard solution		Sample solution		Mean	SD	% RSD
		Intra-day precision	Inter-day precision	Intra-day precision	Inter-day precision			
Aniline (mg L^{-1})	12.0	12.020	12.013	12.051	12.042	12.0315	0.0179	0.149
Benzothiazole (mg L^{-1})	12.0	12.090	12.047	12.100	12.084	12.08025	0.0231	0.191
Nitrite (mg NO$_2$ L^{-1})	0.05	0.0510	0.0490	0.0521	0.0514	0.050875	0.0013	2.614
Nitrate (mg NO$_3$ L^{-1})	1.50	1.5039	1.5010	1.5120	1.5109	1.50695	0.0053	0.354
Chloride (mg Cl L^{-1})	30.0	30.017	30.011	30.029	30.024	30.02025	0.0078	0.026
Total phosphorus (mg P L^{-1})	0.05	0.059	0.053	0.051	0.055	0.0545	0.0034	6.267
Phosphates (mg PO$_4$ L^{-1})	0.10	0.1024	0.1031	0.1015	0.1043	0.102825	0.0011	1.148
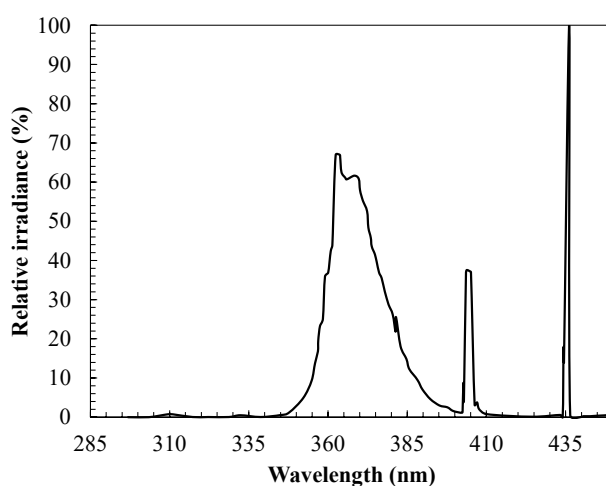
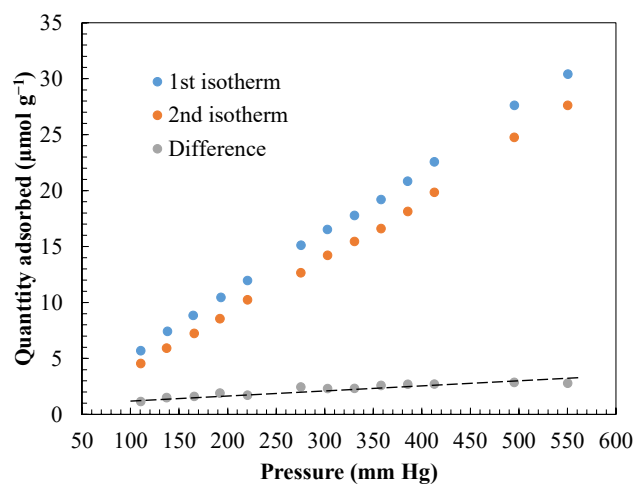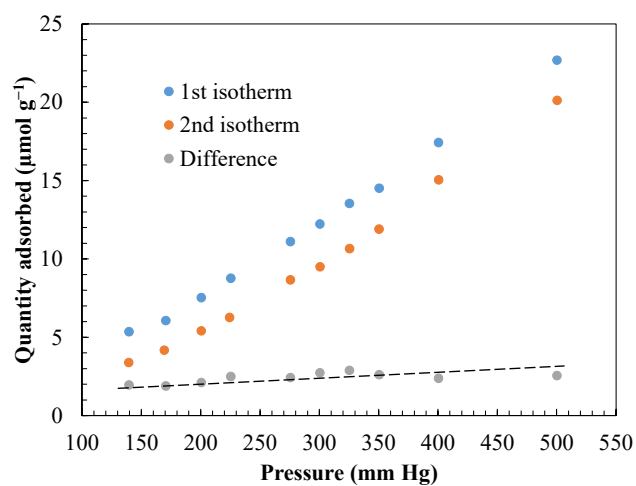**Figure S1.** Spectrum of the UV-A lamp used in the experimental equipment.
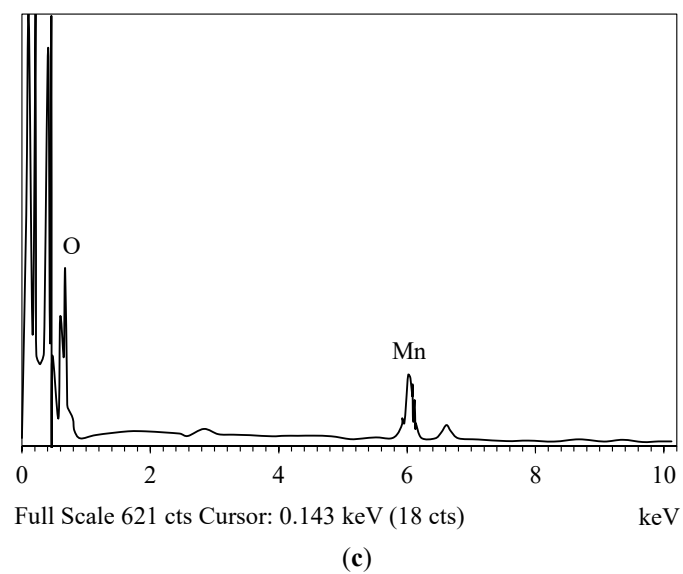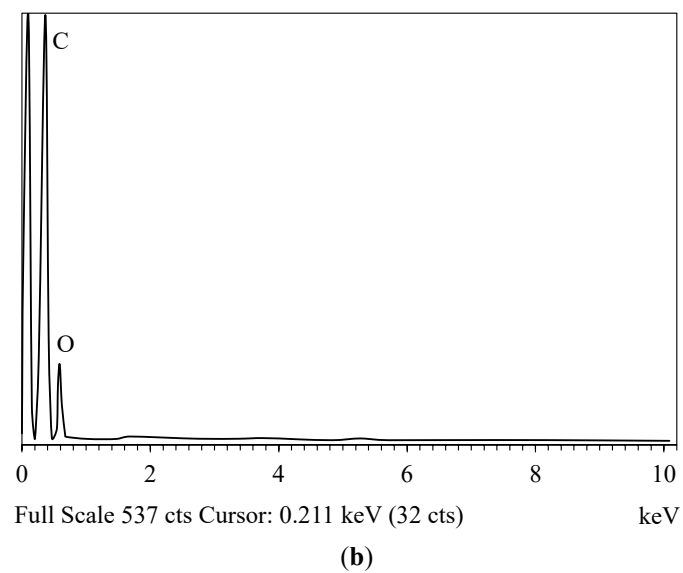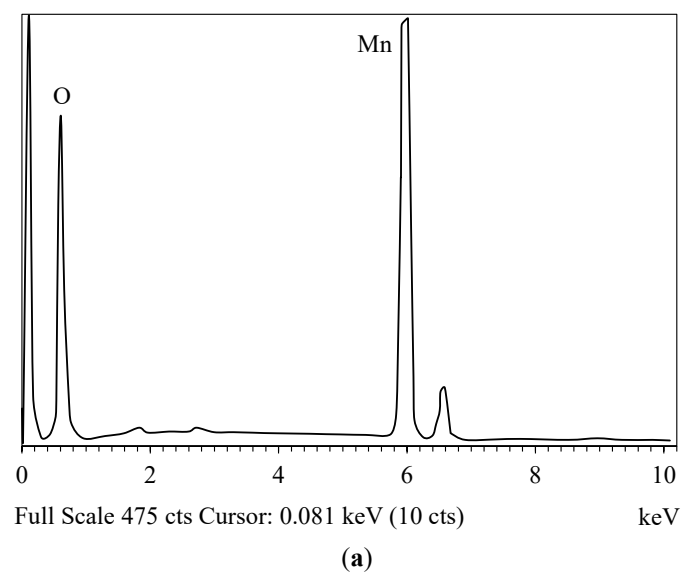
Figure S2. EDX spectra of the materials used in the study: (**a**) synthesised MnO_2 powder; (**b**) Commercial activated carbon Hydrodarco® 3000; (**c**) Synthesized MnO_2/GAC-3 composite.
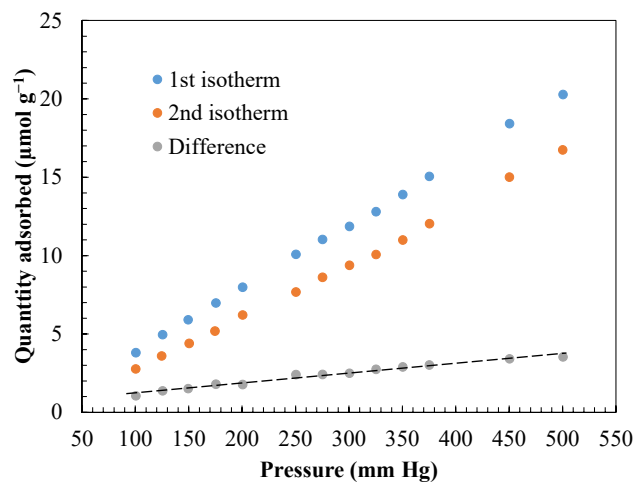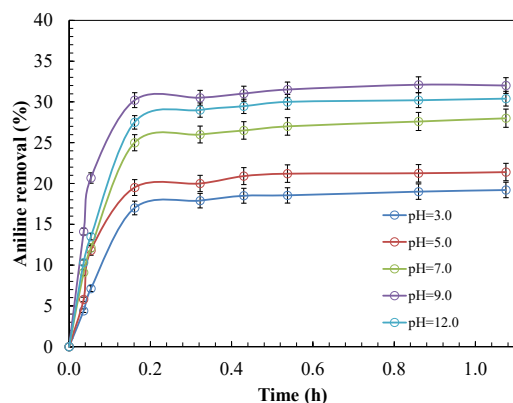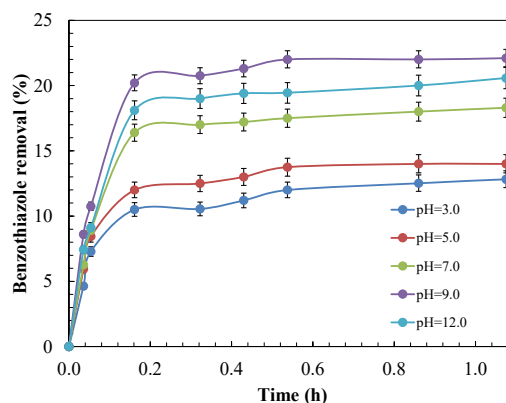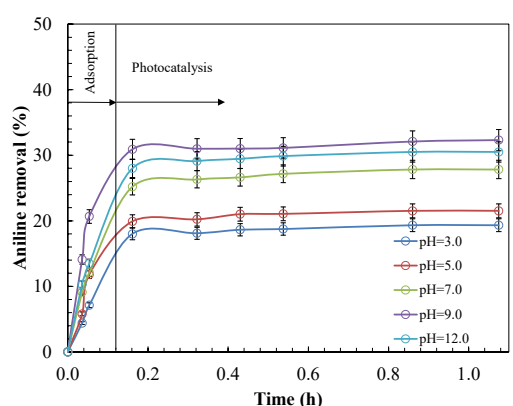
Figure S3. Determination of the H_2 monolayer chemisorbed on the surface of the three MnO_2/GAC composites synthesised in this study: (**a**) MnO_2/GAC-1; (**b**) MnO_2/GAC-2; (**c**) MnO_2/GAC-3.

(**a**)   (**b**)
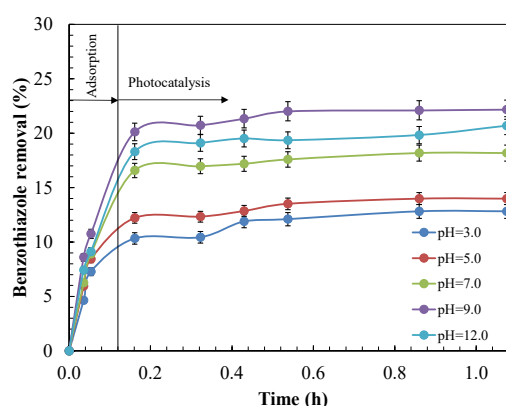
(**c**)   (**d**)
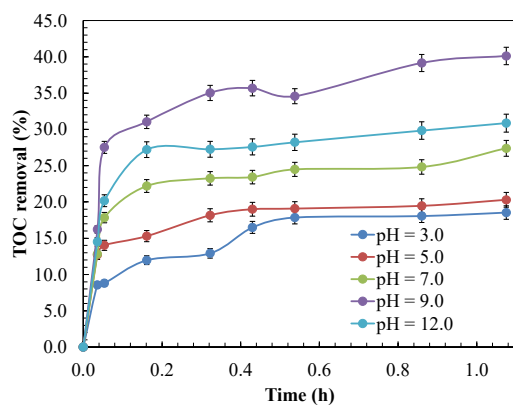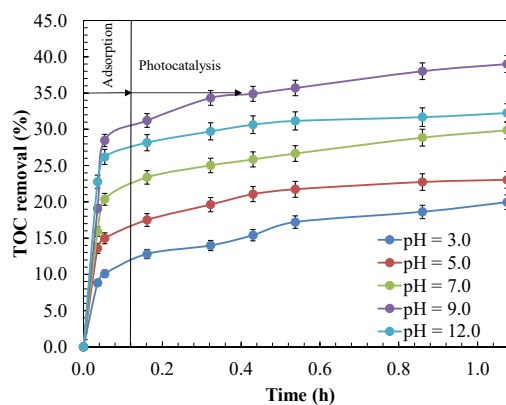
(**e**)   (**f**)

Figure S4. pH effect on the efficiency of the ANI and BTH removal process using GAC Hydrodarco® 3000 during the adsorption and photocatalysis processes. Evolution of the: (**a,b**) Adsorption; (**c,d**) Photocatalysis in primary degradation (**e,f**) and in mineralisation in the adsorption and photocatalysis processes, respectively. Experimental conditions: C_0 = 12.0 mg L⁻¹; m_{CAT} = 0.9 g L⁻¹; *Irradiation dose* = 155.8 W m⁻²; T = 26 °C.
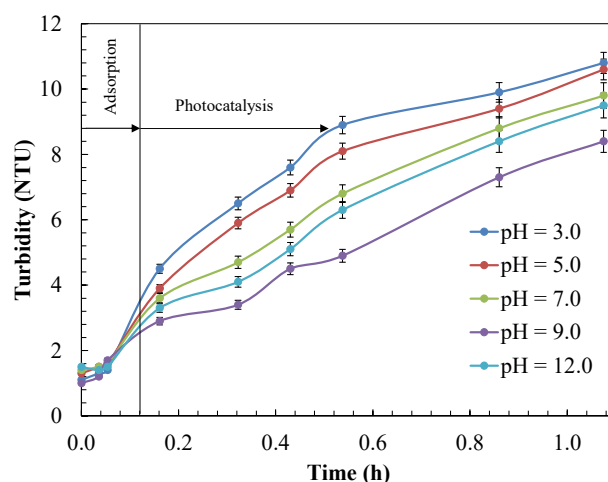
Figure S5. pH effect on turbidity during the photocatalysis of industrial effluents containing ANI and BTH using the GAC Hydrodarco® 3000. Experimental conditions: C_0 = 12.0 mg L^{-1}; m_{CAT} = 0.9 g L^{-1}; *Irradiation dose* = 155.8 W m^{-2}; T = 26 °C.

References

1. Cao, H.; Suib, S.L. Highly Efficient Heterogeneous Photooxidation of 2-Propanol to Acetone with Amorphous Manganese Oxide Catalysts. *J. Am. Chem. Soc.* **1994**, *116*, 5334–5342, doi:10.1021/ja00091a044.

2. Warsi, M.F.; Bilal, M.; Zulfiqar, S.; Khalid, M.U.; Agboola, P.O.; Shakir, I. Enhanced Visible Light Driven Photocatalytic Activity of MnO$_2$ Nanomaterials and Their Hybrid Structure with Carbon Nanotubes. *Mater. Res. Express* **2020**, *7*, 105015, doi:10.1088/2053-1591/abbf8d.

3. Khan, I.; Sadiq, M.; Khan, I.; Saeed, K. Manganese Dioxide Nanoparticles/Activated Carbon Composite as Efficient UV and Visible-Light Photocatalyst. *Environ. Sci. Pollut. Res.* **2019**, *26*, 5140–5154, doi:10.1007/s11356-018-4055-y.

4. Saroyan, H.; Kyzas, G.Z.; Deliyanni, E.A. Effective Dye Degradation by Graphene Oxide Supported Manganese Oxide. *Processes* **2019**, *7*, 40, doi:10.3390/pr7010040.

5. Saroyan, H.S.; Arampatzidou, A.; Voutsa, D.; Lazaridis, N.K.; Deliyanni, E.A. Activated Carbon Supported MnO$_2$ for Catalytic Degradation of Reactive Black 5. *Colloids Surf. A-Physicochem. Eng. Asp.* **2019**, *566*, 166–175, doi:10.1016/j.colsurfa.2019.01.025.

6. Ameta, S. *Advanced Oxidation Processes for Wastewater Treatment: Emerging Green Chemical Technology*; Academic Press, San Diego, CA, USA, **2018**; ISBN 978-0-12-810499-6.

7. Rahmat, M.; Rehman, A.; Rahmat, S.; Bhatti, H.N.; Iqbal, M.; Khan, W.S.; Bajwa, S.Z.; Rahmat, R.; Nazir, A. Highly Efficient Removal of Crystal Violet Dye from Water by MnO$_2$ Based Nanofibrous Mesh/Photocatalytic Process. *J. Mater. Res. Technol.* **2019**, *8*, 5149–5159, doi:10.1016/j.jmrt.2019.08.038.

8. Tang, N.; Tian, X.; Yang, C.; Pi, Z.; Han, Q. Facile Synthesis of α-MnO$_2$ Nanorods for High-Performance Alkaline Batteries. *J. Phys. Chem. Solids* **2010**, *71*, 258–262, doi:10.1016/j.jpcs.2009.11.016.

9. Lin, H.; Chen, D.; Liu, H.; Zou, X.; Chen, T. Effect of MnO$_2$ Crystalline Structure on the Catalytic Oxidation of Formaldehyde. *Aerosol Air Qual. Res.* **2017**, *17*, 1011–1020, doi:10.4209/aaqr.2017.01.0013.

10. Wang, B.; Zhang, H.; Wang, F.; Xiong, X.; Tian, K.; Sun, Y.; Yu, T. Application of Heterogeneous Catalytic Ozonation for Refractory Organics in Wastewater. *Catalysts* **2019**, *9*, 241, doi:10.3390/catal9030241.

11. Farines, V.; Baig, S.; Albet, J.; Molinier, J.; Legay, C. Ozone Transfer from Gas to Water in a Co-Current Upflow Packed Bed Reactor Containing Silica Gel. *Chem. Eng. J.* **2003**, *91*, 67–73, doi:10.1016/S1385-8947(02)00137-7.

12. Urasa, I.T.; Ferede, F. The Determination of Phosphates Using Ion Chromatography: An Evaluation of Influential Factors. *Int. J. Environ. Anal. Chem.* **1986**, *23*, 189–206, doi:10.1080/03067318608076445.